

Component Stress–Strain Behavior and Small-Angle Neutron Scattering Investigation of Stereoblock Elastomeric Polypropylene[†]

Willy Wiyatno and Gerald G. Fuller

Department of Chemical Engineering, Stanford University, Stanford, California 94305-5025

John A. Pople

Stanford Synchrotron Radiation Laboratory, Stanford Linear Accelerator Center, Stanford University, Stanford, California 94309

Alice P. Gast

Department of Chemical Engineering, Massachusetts Institute of Technology, Cambridge, Massachusetts 02139-4307

Zhong-ren Chen and Robert M. Waymouth*

Department of Chemistry, Stanford University, Stanford, California 94305-5080

Charles L. Myers

BP Chemical Company Research Center, Naperville, Illinois 60566

Received March 25, 2002; Revised Manuscript Received November 18, 2002

ABSTRACT: Elastomeric polypropylene (ePP) produced from unbridged 2-arylidene metallocene catalysts was studied by uniaxial tensile and small-angle neutron scattering (SANS) techniques. The ePP can be separated into the following: a low tacticity fraction soluble in ether (ES), an intermediate tacticity fraction soluble in heptane (HS), and a high tacticity fraction insoluble in heptane (HI). Tensile properties of ePP were compared to its solvent fractions, and the role of each solvent fraction residing within ePP was investigated by blending 5 wt % deuterated fraction with ePP. The tensile properties of each fraction vary considerably, exhibiting properties from a weak gum elastomer for ES, to a semicrystalline thermoplastic for HI. The intermediate tacticity HS fraction exhibits elastic properties similar to the parent elastomer (ePP). In the melt at 160 °C, SANS shows that all deuterated fractions are homogeneously mixed with ePP. Slow cooling from the melt to 25 °C causes the low tacticity fraction to preferentially segregate in amorphous domains due to different crystallization temperatures and kinetics although, despite its low crystallinity ($\leq 2\%$), the low tacticity fraction can cocrystallize with the matrix. The dES-ePP shows little or no relaxation when held under strain and recovers readily upon the release of stress. The high tacticity component (dHI-ePP) retains its plastic properties in the blend.

Introduction

Isotactic polypropylene (i-PP) is a low-cost semicrystalline thermoplastic exhibiting excellent mechanical properties with a worldwide production exceeding 20 million metric tons.¹ The crystallinity of isotactic PP is a consequence of the regular structure of the stereogenic centers along the polymer backbone; in contrast atactic polypropylene is an amorphous material. Natta was the first to isolate an elastomeric form of polypropylene and attributed the novel properties to a multiblock microstructure comprising alternating sequences of isotactic and atactic sequences.^{2,3}

Elastomeric polypropylenes (ePP) can be produced by a number of different synthetic strategies.^{4–11} More recently, several classes of metallocene catalysts have been developed for the production of elastomeric polypropylenes,^{12–20} notably those developed by Chien,^{21–25} Collins,^{26–28} Rieger,^{29,30} Erker,³¹ and our group.^{32–51} The structures and properties of the elastomeric polypropylenes produced from from unbridged 2-arylidene metallocene catalysts^{32–51} are compositionally heterogeneous and can be separated into fractions of different

tacticity, crystallinity, and molar mass.^{33,39} Successive boiling-solvent extraction yields three fractions: a low tacticity ether-soluble fraction (ES), an intermediate tacticity heptane-soluble fraction (HS), and a high tacticity heptane-insoluble (HI) fraction.

The compositional heterogeneity of these materials is likely to impact their properties, but the role of each solvent fraction on the overall properties of elastomeric polypropylenes is not well-established.^{4–7} In this study, we report the tensile properties of a sample of ePP and its solvent fractions at room and elevated temperatures. The deformation behavior of the individual fractions when dispersed in the ePP matrix is studied by labeling the individual fractions with deuterium and investigating the arrangement and deformation behavior of the labeled chains under strain^{52–54} by small-angle neutron scattering (SANS). The miscibility of the deuterated components in ePP was examined in the melt and in the crystalline state. We relate the degree of chain orientation to both the chain tacticity and the applied deformation through observations of the anisotropy of the neutron-scattering profiles. The current experiments complement previous studies on the dynamic response of each solvent fraction under a tensile deformation using rheo-optical and X-ray scattering methods.^{46,55}

[†] Work supported by the U.S. Department of Energy, Contract DE-AC03-76SF00515.

Table 1. Polymer Characteristics and Physical Properties

sample	wt %	M_n^a (kg/mol)	M_w/M_n^a	[mmmm]	[m] (%) ^b	IR index ^c	T_m (°C) ^d	ΔH (J/g) ^d	crystallinity (%)	
				(%) ^b					DSC	XRD
ePP-10	100	87	2.3	34	73	0.34	42–149	22	11	8
ES-ePP10	48	70	2.1	21	67	0.19	41–45	2	1	2
HS-ePP10	42	96	2.3	44	79	0.38	42	32	15	11
HI-ePP10	10	173	2.5	76	92	0.70	47–155	82	39	37
ePP-10 annealed							50–160	27	14	

^a Determined by GPC (waters 150 °C) at BP Chemical Co. ^b Determined by ¹³C NMR, [mmmm] is fraction of five contiguous isotactic sequences. ^c Determined by the ratio of absorbance intensity A_{998}/A_{975} . ^d Determined by DSC endotherm scan from 0 to 200 °C at 20 °C/min.

Experimental Section

Sample Preparation. Elastomeric polypropylene (ePP-10) was synthesized at BP Chemical Co. in liquid propylene at 50 °C with bis(2-(3,5-di-*tert*-butylphenyl)indenyl) hafnium dichloride/MAO catalyst systems, as reported elsewhere.⁵⁶ Boiling-solvent fractionation was carried out following the procedure described earlier^{33,39,56} with boiling diethyl ether and heptane to yield a low tacticity ether-soluble (ES) fraction, an intermediate tacticity heptane-soluble (HS) fraction, and a high tacticity heptane-insoluble (HI) fraction. Table 1 shows the physical properties of the materials.

Deuterated polypropylene was prepared following conditions as closely as possible to those of PP1 reported previously.³⁹ Deuterated monomer (C₃D₆) from Cambridge Isotopes was purified by condensing about 30 mL of deuterated monomer into a lecture bottle containing 2 g of solid methylaluminoxane (MAO), obtained by vacuum-drying of a toluene MAO solution (Akzo MAO type 4). The deuterated propylene was then recondensed into the original container and the process repeated to remove all impurities. Polymerization was carried out in a 300-ml Parr reactor equipped with a mechanical stirrer equilibrated at 20 °C with an ethylene glycol/water cooling-loop. The reactor was flushed three times with argon and toluene, and half of the MAO was injected as a toluene solution under argon. The reactor was cooled with a dry ice/acetone bath, and the purified deuterated propylene condensed into the reactor. The reactor was warmed slowly to room temperature, and a catalyst solution of bis(2-phenylindenyl)-zirconium dichloride,³⁹ previously activated with the remaining half of the MAO, was injected as a toluene solution under argon pressure. A total of 25 mL of toluene and 25 mL of propylene were used for each polymerization with catalyst concentration of 5×10^{-5} M and the [MAO]/[Zr] ratio of 3500. Polymerization ran for 1 h and the excess deuterated monomer recondensed into the lecture bottle. Polymer from the reactor was precipitated into acidified methanol with 5% HCl. After stirring for 1 day, the polymer was washed with pure methanol for another 12 h, and the polymers collected and dried in a vacuum oven at 40 °C for at least 1 day. GPC analysis of molecular weight indicated $M_n = 129$ kg/mol and $M_w/M_n = 5.5$. ²H-decoupled ¹³C NMR analysis indicated an isotacticity content of [mmmm] = 30%.

Samples for SANS experiments were prepared by blending 5% (by weight) of the deuterium labeled fraction with protonated ePP-10. The perdeuterated polymer (d-ePP) sample was fractionated by successive extraction with boiling diethyl ether and heptane under a nitrogen atmosphere following the same procedure as for the protonated ePP-10. Each deuterated fraction (d-ePP, d-ES, d-HS, or d-HI) and protonated ePP-10 was dissolved in boiling xylene (300 mL) in the presence of 0.2wt % antioxidant 2,6-di-*tert*-butyl-4-methylphenol (BHT). Polymer blends were precipitated into methanol with vigorous stirring. The resulting blends were dried at 40 °C in a vacuum and hot-pressed to a thickness of 0.5–1.0 mm at 180 °C between two Teflon sheets (Mechanical Grade PTFE, McMaster-CARR) and ambiently cooled to room temperature.

Material Characterization. Number and weight-average molecular weights (M_n and M_w) were obtained at BP Chemical Co. using a Waters 150C high-temperature chromatograph. The solvent used was 1,2,4-trichlorobenzene at 139 °C using

two Polymer Laboratories PL GEL Mixed-B columns at a flow rate of 1 mL/min. The samples were calibrated against polypropylene standards.

The ²H-decoupled ¹³C NMR spectra of the perdeuterated polypropylene were obtained at the Varian Applications Lab. For protonated polypropylenes, ¹³C NMR spectra were recorded at 75.425 MHz on a Varian UI 300 spectrometer at 100 °C using 10 mm sample tubes. Samples were prepared in 1,1,2,2-tetrachloroethane containing about 0.5 mL of 1,1,2,2-tetrachloroethane-*d*₂.⁵⁵

Thermal analysis was performed using a Perkin-Elmer DSC 7 with indium as a calibration standard. Polymer samples (about 0.01 g) were melt-pressed between two Teflon sheets (Mechanical Grade PTFE, McMaster-CARR) at 180 °C using a light pressure (≤ 250 psig). Disklike samples were punched from films cooled with liquid nitrogen using a standard one-hole paper punch. These samples were weighed and sealed into an aluminum DSC pan supplied by Perkin-Elmer. Samples were pretreated from room temperature to 200 °C at 20 °C/min, held at 200 °C for 10 min, cooled to room temperature at 20 °C/min, and then aged at room temperature for 24 h. The melting temperature and the heat of fusion were measured by heating from –50 to +200 °C at 20 °C/min. Crystallinity was calculated by normalizing the heat of fusion (ΔH_f) from the endotherm scans by a theoretical value of a completely crystalline sample of 209 J/g.⁵⁷

Tensile Tests. Tensile tests were performed with ASTM D-1708 dumbbell specimens (2.2 cm gauge length) die cut from compression-molded sheets with a thickness of about 0.5 mm. Room-temperature tensile tests were performed at BP Chemical Co. with a crosshead separation rate of 25.4 cm/min. Temperature-dependent tensile tests were conducted with a Miniature Material Tester, MiniMat 2000 (Rheometric Scientific, Inc.) with a crosshead separation rate of 10 mm/min. The tensile modulus was determined as the tangent slope at the lowest strain. Hysteresis cycle tests were performed by elongating the specimen to 100% elongation ($2 \times$ original gauge length) in three successive cycles, with 30 s hold at 100% elongation and 60 s hold after crosshead recovery between cycles. Stress relaxation is measured as the decrease in stress during extension at 100% elongation for 30 s. Retained force was measured as the ratio of stress at 50% elongation during the recovery step to the initial stress at 100% elongation in the second cycle. A three-cycle recovery test was performed by elongating the specimen to 300% elongation ($4 \times$ original gauge length) with no hold time imposed at extension; crosshead direction was immediately reversed after reaching 300% elongation. The elongation at which stress returned to the baseline identified a tensile set for the first cycle. A tensile set for the second cycle was the elongation at which stress exceeded the baseline during the extension. Hysteresis-to-break tests were conducted by successive cycles of increasing elongations to 300%, 500%, and 700% and finally to the break of the specimen. In each cycle, the specimen followed a recovery step with no holding at strain.

Small-Angle Neutron Scattering (SANS). SANS was performed at the National Institute of Standards and Technology (NIST) Center for Neutron Research (NCNR) in Gaithersburg, MD. SANS for samples in the melt at 160 °C and under strain at room temperature were performed on beam-

lines NG1 and NG3, respectively. The neutron beam was ~ 6 mm in diameter and of incident wavelength $\lambda = 6$ (strain experiments) and 9 \AA (melt experiments). The energy resolution of the source was $\Delta\lambda/\lambda \sim 0.15$. For the melt experiments the samples were placed in a cell with copper windows and for the strain experiments samples were held with a tensile testing device and had an initial active path length of 1.0 – 1.2 mm. Data were collected on a 2-D multiwire detector providing the following q range: $0.002 \text{ \AA}^{-1} < q < 0.05 \text{ \AA}^{-1}$ (where q is the following scattering vector: $q = 4\pi(\sin \theta)/\lambda$ for a radiation of wavelength λ scattered through an angle 2θ). Each exposure was collected over a 20-min period. These data were corrected for background scattering and scattering from the relevant windows and normalized for the proportion of scattering volume intersecting the probe beam. Incoherent background scattering was subtracted from scattering of the fully protonated sample. The patterns from the stretched, tagged polypropylene samples were normalized with the SANS pattern from the untagged matrix at the same extension ratio in an effort to counteract incoherent scattering. True strain (ϵ) was calculated from the ratio of the change in separation distance between two lines drawn at the middle of the specimen ($\Delta l = l - l_0$) to its original separation distance (l_0): $\epsilon = \Delta l/l_0$. The tensile testing device was repositioned in the beam so that the probe beam always impinged on the vertical center of the sample after stretching.

Data Analysis

Analysis of SANS. Analysis of polymer compatibility of the deuterated fraction within ePP was derived from the Zimm analysis of polymer blends originally developed for light and small-angle X-ray scattering. The coherent cross section ($d\Sigma/d\Omega$) of a homogeneous blend of two polymer species, one of which is deuterium labeled, is^{58–60}

$$\frac{d\Sigma}{d\Omega} = (a_H/v_H - a_D/v_D)^2 S(q) \quad (1)$$

where a_D and a_H are the scattering lengths of the repeat units (monomers) of the labeled and unlabeled species, which have the specific molar volumes of v_H and v_D , respectively. Assuming that the polymer chains form ideal (Gaussian) conformations which are unperturbed by the weak interactions between monomers, the structure factor $S(q)$ based on the random phase approximation (RPA) is⁶¹

$$\frac{1}{S(q)} = \frac{1}{v_H N_{w,H} \phi_H P_H(q^2 R_{g,H}^2)} + \frac{1}{v_D N_{w,D} (1 - \phi_H) P_D(q^2 R_{g,D}^2)} - \frac{2\chi_{HD}}{v_0} \quad (2)$$

where $N_{w,D}$, $N_{w,H}$, $R_{g,D}$, and $R_{g,H}$ are weight-averaged degree of polymerization and z -average radii of gyration of the labeled and unlabeled species, respectively. The volume fraction of the unlabeled species is denoted by ϕ_H and the reference volume is defined as $v_0 = (v_H v_D)^{1/2}$. The Flory–Huggins interaction parameter between segments of the labeled and unlabeled species is represented by χ_{HD} . The intrachain functions $P_H(q^2 R_{g,H}^2)$ and $P_D(q^2 R_{g,D}^2)$ are represented by a z -averaged Gaussian (Debye) function.^{62,63}

At small scattering vector q , eqs 1–2 reduce to the Ornstein–Zernike or Zimm form^{64,65}

$$\frac{d\Sigma}{d\Omega}(q) = \frac{\frac{d\Sigma}{d\Omega}(0)}{1 + q^2 \xi^2} \quad (3)$$

$$\frac{d\Sigma}{d\Omega}(0) = \frac{((a_H/v_H) - (a_D/v_D))^2}{(v_H N_{w,H} \phi_H)^{-1} + (v_D N_{w,D} \phi_D)^{-1} - 2(\chi_{HD}/v_0)} \quad (4)$$

where ξ is the composition fluctuation correlation length. The correlation length is a measure of distance over which the concentration fluctuations remain correlated and can be obtained from the slope and extrapolated intercept of the graph $(d\Sigma/d\Omega)^{-1}$ vs q^2 .

We describe molecular anisotropy following the approach outlined by Mitchell and Windle.⁶⁶ Molecular orientation is described by the azimuthal coherent cross section averages of the second spherical harmonic component of a uniaxial distribution function:

$$P_2(\cos\alpha) = \frac{3 \cos^2\alpha - 1}{2} \quad (5)$$

where α is the angle between the polymer coil and the orientation director vector (uniaxial extension axis). The orientational parameter (S) is represented in terms of the normalized amplitudes of the spherical harmonics:

$$S = \frac{\langle P_2(\cos\alpha) \rangle_{\text{sample}}}{\langle P_2(\cos\alpha) \rangle_0} \quad (6)$$

where $\langle P_2(\cos\alpha) \rangle_{\text{sample}}$ is calculated by

$$\langle P_2(\cos\alpha) \rangle = \frac{\int_0^{\pi/2} \frac{d\Sigma}{d\Omega}(q,\alpha) P_2(\cos\alpha) \sin\alpha \, d\alpha}{\int_0^{\pi/2} \frac{d\Sigma}{d\Omega}(q,\alpha) \sin\alpha \, d\alpha} \quad (7)$$

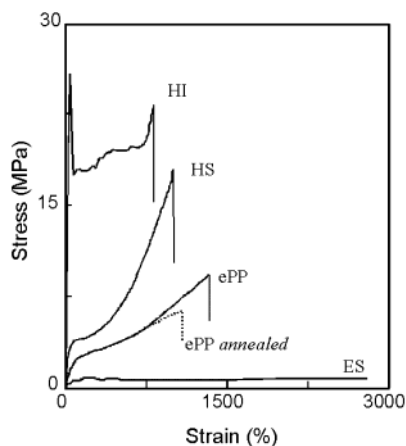
where $d\Sigma/d\Omega(q,\alpha)$ is the scattering cross section azimuthal average of the scattering patterns. The model for a single unit is assumed to be an infinitely long rod, (in physical terms, assumes as stiff chain with an infinitely high M_w), so that the orthogonal components of the scattering model are $\langle P_2(\cos\alpha) \rangle_0 = -1/2$. The integration limits indicate that a complete description of the orientation function can be obtained from a single quadrant of a scattering pattern: the results presented here are determined from the complete azimuthal range of $0 < \alpha \leq 2\pi$, averaged over the four quadrants.

Modeling the scattering unit as an infinitely long, rigid rod introduces degrees of uncertainty into the orientation measurements, as the scattering units in this case are semiflexible polymer chains of finite length. Nevertheless this analysis has been used successfully to characterize short rigid rod systems⁶⁷ (nematic liquid crystal systems) as well as elastomeric systems⁶⁸ and linear polymer melts.⁶⁹ This system, an elastomeric polymer, comprises semiflexible chains that will adopt different degrees of orientation at different length scales. This is evidenced by differing radial anisotropy profiles as a function of the reciprocal space vector. Additionally the orientation function is characterized here only by the first nonzero order coefficient of the

Table 2. Tensile Properties of EPP-10 and Its Solvent Fractions

sample	ePP-10	ES-ePP10	HS-ePP10	HI-ePP10	ePP-10 (annealed)
density (g/cm ³)	0.863	0.859	0.877	0.913	0.862
tensile strength (MPa)	8.01	0.81	18.2	26.1	6.07
tensile modulus (MPa)	6.28	1.73	19.5	259	8.94
elongation to break (%)	1305	>3,000	994	690	1100
tensile stress relaxation ^a (%)	47.3	41.6	38.7	n.o. ^b	48.2
retained force, 50% recovery ^c (%)	10.6	18	26.5	n.o. ^b	5.4
recovery tests ^d					
tensile set first cycle ^e (%)	58	53	35	n.o. ^b	65
tensile set second cycle ^f (%)	17	6	15	n.o. ^b	29

^a Decrease in stress (or force) during 30 s the specimen is held at 100% elongation. ^b Not observed, exhibits plastic deformation. ^c Ratio of stress at 50% elongation during recovery to stress at 100% elongation at the 2nd cycle. ^d Three extension cycles to 300% with no holding time at extension. ^e Elongation at which stress returns to the baseline after 300% elongation. ^f Elongation at which stress increases above the baseline.

**Figure 1.** Tensile properties of ePP-10 and its solvent fractions.

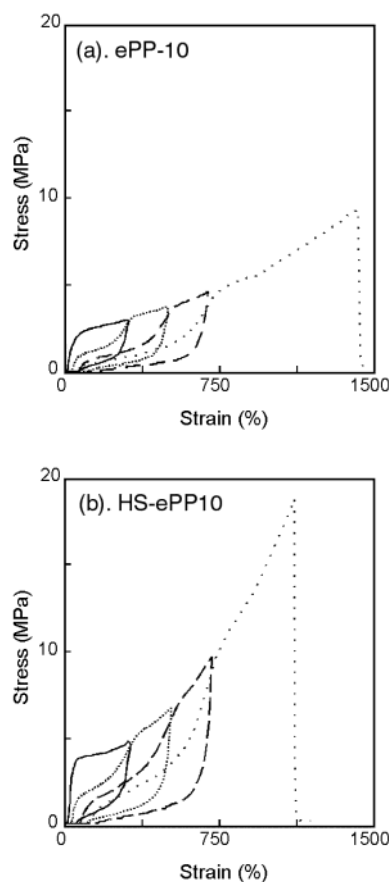
Legendre polynomial series, $\langle P_2 \rangle$; thus, orientation measurements presented here are only first-order quantifications of the macromolecular response of the bulk material to the applied deformation.

Results and Discussions

Mechanical Properties. The physical properties of ePP-10 are tabulated in Tables 1–3.⁵⁶ The tensile behavior of ePP-10 and its solvent fractions are illustrated in Figures 1 and 2 and summarized in Tables 2 and 3. Elastomeric polypropylene (ePP-10) exhibits tensile properties characteristic of a polyolefin thermoplastic elastomer: a high (1300%) elongation at break, a tensile strength of 8 MPa, good elastic recovery as measured by a moderate tensile set of 58% following a 300% elongation, and stress–strain hysteresis. For ePP-10, 47% of the engineering stress decays within 30 s at 100% elongation.

The tensile properties of the fractions obtained from boiling-solvent extraction vary considerably. The HI fraction exhibits properties typical of a semicrystalline thermoplastic, deforming irreversibly with necking behavior typical of isotactic PP (Table 1). The HS fraction is elastomeric and exhibits a higher tensile strength and modulus than the whole polymer; this is consistent with its higher tacticity, density, and heat of fusion.⁷⁰ The ES fraction exhibits properties of a weak gum elastomer with a low tensile modulus and strength, but a tensile set comparable to ePP-10 (Table 2). The stress relaxation for both the ES (42%) and HS fractions (39%) are similar to that of ePP-10.

To investigate the effect of thermal history on the mechanical properties, a compression-molded sample of

**Figure 2.** Hysteresis curves of ePP-10 and the intermediate tacticity heptane-soluble (HS) fraction.**Table 3. Temperature-Dependent Tensile Properties**

sample	[<i>mmmm</i>] (%)	temp (°C)	tensile modulus (MPa)	tensile set ^a (%)
ePP-10	34	25	11.8 ± 0.8	17.1 ± 1.0
ePP-10	34	50	5.8 ± 1.1	28.3 ± 1.1
HS-ePP10	44	25	19.6 ± 0.6	12.2 ± 0.1
HS-ePP10	44	50	7.4 ± 0.2	19.6 ± 0.9

^a Elongation at which stress returns to the baseline after 100% elongation.

ePP-10 was annealed isothermally at 160, 155, and 150 °C for 24 h successively and then annealed for 12 h subsequently at progressively lower temperatures in 10 °C increments. The tensile properties of this sample were compared to a compression-molded sample cooled slowly from the melt (at approximately 5 °C/min); but no strong influence of the previous thermal history was found.⁷¹ The tensile properties of annealed ePP-10 are

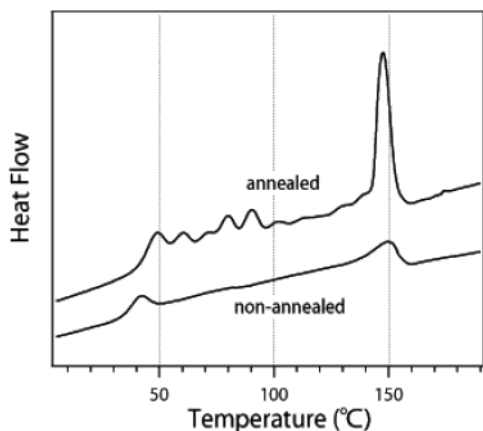


Figure 3. Effect of thermal history on the melting profile of elastomeric polypropylene ePP-10 as measured by DSC. Reprinted from ref 56. Copyright 2002 American Chemical Society.

similar to the nonannealed compression-molded sample; the elongation to break is somewhat less (1100%) and the retained force at 50% recovery is lower, but other tensile properties are not significantly different from the compression-molded sample (Table 2). These results are surprising since in studies reported elsewhere,^{56,72} we have shown that both the melting profiles (Figure 3) and the crystalline morphologies of ePP-10 (studied by tapping mode AFM) depend strongly on the thermal history. The melting profile of the nonannealed sample reveals a broad melting range extending up to 160 °C, with two melting peaks centered at 40 and 150 °C. The annealed sample, on the other hand, shows a narrow high-temperature melting peak centered at 149 °C, as well as a distribution of melting peaks from 40 to 100 °C. While the distribution of melting peaks is quite different, the degrees of crystallinity are not strongly influenced by annealing, as manifest in similar heats of fusion (Table 1). Morphological studies reveal large hierarchical hedritic morphologies for samples annealed at 120–130 °C.⁷² While morphological studies were not carried out on annealed samples used for tensile tests, these results imply that the tensile properties are determined to first order by the total degree of crystallinity rather than the specific morphological features observed. Further studies are warranted to investigate the influence of thermal history and morphology on the properties of these materials.

Stress–strain hysteresis is a characteristic feature of polyolefin thermoplastic elastomers. In Table 2, hysteresis is reported as tensile stress relaxation and retained force. The stress relaxation of 47–48% is similar for annealed and nonannealed samples of ePP-10 at 100% elongation, whereas the retained force is lower for the annealed sample. A tensile recovery test on ePP-10 and the HS fraction reveals a higher degree of hysteresis for HS (Table 2 and Figure 2). We had envisioned that the presence of a significant amount (48%) of the low-crystallinity ES fraction in ePP-10 might be a source of the stress relaxation in ePP-10. However, the higher degree of hysteresis for the HS fraction (from which all the ES fraction has been removed) relative to ePP-10 implies that the ES fraction is not the sole or even primary source of stress relaxation in ePP-10. Our current hypothesis, which is partially supported from rheo-optical studies of the relaxation properties,^{47,55} is that amorphous segments of chains partially tethered with the crystallites act as a primary source of stress

Table 4. Polymer Characteristics in SANS Studies

sample	wt %	M_n^a (kg/mol)	M_w/M_n^a	$[mmmm]$ (%) ^b	T_m (°C) ^c	ΔH (J/g) ^c
d-ePP	100	129	5.5	30	30–147	13
d-ES	34	87	3.6	18 ^d		0
d-HS	42	129	3.7	33 ^d	35–140	18
d-HI	24	186	6.3	51 ^d	30–155	50

^a Determined by high-temperature GPC at BP Chemical Co. ^b Determined by ¹³C NMR, fraction of five contiguous isotactic sequences. ^c Determined by DSC, endotherm scans from –50 to +200 °C at 20 °C/min. ^d Values estimated from protonated fractions prepared and fractionated under similar conditions.³⁹

relaxation. It is highly unlikely that every chain ends or begins with a crystallizable isotactic sequence, and thus atactic chain sections that are only partially constrained in crystallites provide a mechanism for relaxation after deformation.

A series of tensile measurements were carried out at both 25 °C and 50 °C in a temperature-controlled Minimat Tensile Testing device to assess the temperature dependence of tensile properties (Table 3). These experiments were carried out with a crosshead separation of 10 mm/min, different than those reported in Table 2, but the moduli and tensile sets of ePP-10 and HS-ePP10 are roughly comparable to those reported in Table 2. Temperature dependence experiments reveal that both ePP-10 and HS retain elastomeric properties at 50 °C, although the moduli decrease by a factor of 2 and the tensile sets increase by approximately 60%. The tensile set in these temperature-dependent studies is measured after 100% elongation, rather than the 300% elongation used in the studies in Table 2.

Deuterated ePP. A sample of deuterated ePP was prepared and fractionated in order to probe the molecular orientation of deuterated ePP chains under strain. The characterization of deuterated ePP and its solvent fractions is given in Table 4. The tacticity of deuterated ePP (d-ePP), reported as the fraction of isotactic $[mmmm]$ pentads, is $[mmmm] = 30\%$, similar to that of ePP-10 ($[mmmm] = 34\%$).^{56,72} The number-average molecular weights are comparable (d-ePP $M_n = 129$ kg/mol vs ePP-10 $M_n = 87$ kg/mol), but the molecular weight distribution of the deuterated d-ePP was broader at $M_w/M_n = 5.5$. The melting point and heat of fusion of d-ePP are $T_m = 128$ °C and $\Delta H = 13$ J/g, respectively. These values are lower than those of the protonated samples, but within the range of elastomeric polypropylenes we have tested previously.^{39,56,72} Fractionation of d-ePP was carried out under similar conditions to that of ePP-10. The properties of the deuterated fractions are comparable, although not identical to those of ePP-10 (Tables 1 and 4). Fractionation of d-ePP generated slightly less weight percent of an ES fraction, comparable amounts of the HS fraction, and slightly more of an HI fraction compared to ePP-10 (Tables 1 and 4).

Small-angle neutron scattering (SANS) was carried out on a series of samples of ePP-10 doped with 5 wt % of a deuterated ePP or its fractions. The 1-D SANS coherent cross section profiles of ePP-10 doped with the deuterated high-tacticity fraction (dHI-ePP) in the melt at 160 °C and crystalline state at 25 °C are shown in Figure 4. The scattering profiles in the crystalline state are slightly lower than those at 160 °C at high q region, but otherwise the profiles at 160 and 25 °C are comparable over the range of q investigated. Fitting the data with eqs 1 and 2, assuming a random phase approximation (RPA) function, yields a good data regression. The

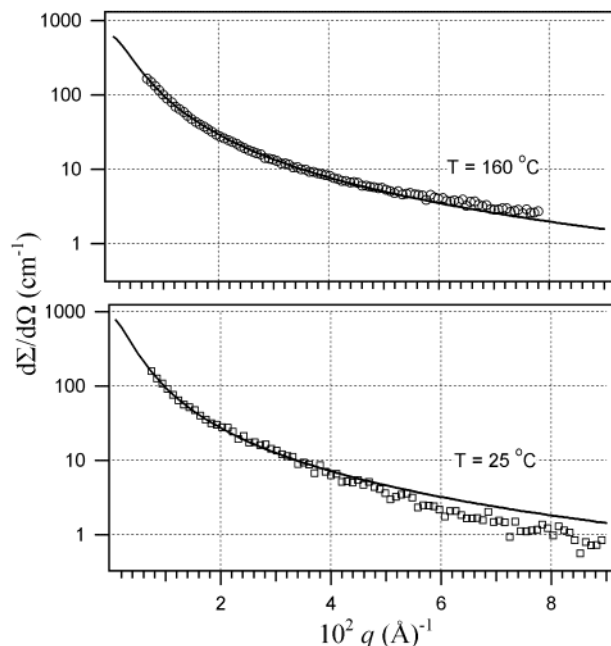


Figure 4. 1-D SANS coherent cross section profiles of high tacticity heptane-insoluble fraction within ePP (dHI-ePP) in the melt (160 °C) and crystalline (25 °C) state.

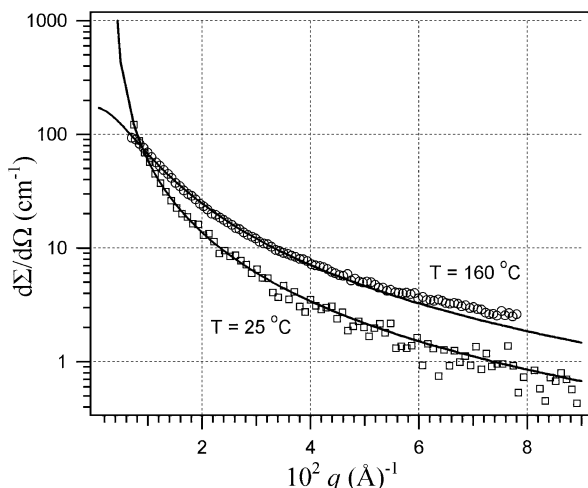


Figure 5. 1-D SANS coherent cross section profiles of low tacticity ether-soluble fraction within ePP (dES-ePP) in the melt (160 °C) and crystalline (25 °C) state.

similarity of the scattering profiles and their conformance to the RPA model imply that dHI fraction is miscible and well-dispersed in ePP-10, and there is only a slight change in the conformation of the dHI-ePP fraction upon crystallization from the melt.

Similar experiments carried out with ePP-10 doped with 5 wt % dES-ePP revealed quite a different behavior. The scattering profiles of dES-ePP at 160 °C are similar to those of dHI-ePP and conform reasonably well to the RPA model; thus, we conclude that the d-ES chains are equally well dispersed in ePP-10 (vide infra). In contrast, the scattering profile for dES-ePP at 25 °C is quite different (Figure 5); the cross sections decay steeply with q in the low q region ($q \leq 0.015$ Å) and are much lower than those at 160 °C at higher scattering vectors ($q \geq 0.01$ Å). The latter observation suggests that the deuterated chains are not homogeneously mixed at 25 °C. For mixtures with the same composition, Alamo and co-workers calculated that scattering

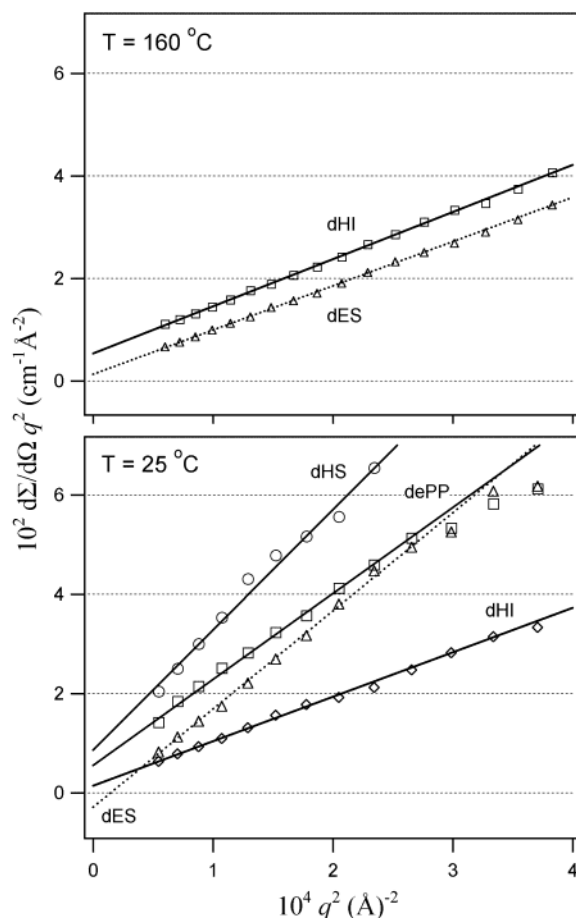


Figure 6. Ornstein-Zernike or Zimm plots of deuterated fractions within ePP in the melt (160 °C) and crystalline (25 °C) state.

Table 5. SANS Molecular Characteristics in Melt at 160 °C

sample	$\chi_{HD}^d \times 10^4$	$\chi_{HD-critical}^a \times 10^4$	$d\Sigma/d\Omega(0)_{exp}$ (cm ⁻¹)	$d\Sigma/d\Omega(0)_{calc}^{a,b}$ (cm ⁻¹)
dES-ePP	1.4	14.4	185	167
dHI-ePP	1.4	4.7	765	533

^a Specific molar volumes of deuterated fractions are estimated from those of protonated fractions. ^b Ideal mixing system with Flory-Huggins interaction parameter $\chi_{HD} = 0$.

cross sections for a two-phase polymer melt are lower than those of a one-phase system at high q .⁷³

Analysis of the scattering data of the deuterated samples according to the Ornstein-Zernike (OZ) or Zimm analysis (eqs 3 and 4) in a low q region provided further information. All labeled fractions within ePP show a linear dependence of $(d\Sigma/d\Omega)^{-1}$ vs q^2 at low scattering vector ($q \leq 0.02$ Å) (Figure 6). In the melt at 160 °C, the OZ plots of dHI-ePP and dES-ePP extrapolate to positive intercepts, suggesting a homogeneity where the deuterated fractions are miscible with ePP in the melt.^{64,65} Extrapolation of the OZ plots to $q = 0$ yields cross sections $d\Sigma/d\Omega(0)$ of 765 and 185 cm⁻¹ for dHI-ePP and dES-ePP, respectively. The calculated cross sections for an ideal mixing case ($\chi_{HD} = 0$) are 533 and 167 cm⁻¹ for dHI-ePP and dES-ePP, respectively. The Flory-Huggins interaction parameters calculated from the OZ plots are identical for both systems, $\chi_{HD} = 1.4 \times 10^{-4}$, but smaller than the critical interaction parameter χ_s (Table 5). The interaction parameter for a regular homogeneously mixed polyolefin blend is

usually between the athermal limit and stability limit: $0 \leq \chi \leq \chi_s$,⁶¹ the stability limit is given by

$$\chi_s = \frac{v_0}{2} \left(\frac{1}{v_H N_{w,H} \phi_H} + \frac{1}{v_D N_{w,D} \phi_D} \right) \quad (8)$$

The OZ plot analysis indicates that both dHI-ePP and dES-ePP are homogeneously mixed in the melt at 160 °C without clustering or aggregation of the labeled chains.

In the crystalline state at 25 °C, the Ornstein–Zernike plots yield positive extrapolated intercepts for dePP-ePP, dHS-ePP, and dHI-ePP (Figure 6) that suggest a homogeneous one-phase system, but the OZ plot of dES-ePP extrapolates to a negative intercept. This suggests that the d-ES chains are not homogeneously well-mixed within the crystallized ePP matrix. There are two possibilities: either the d-ES fraction does not cocrystallize at all or it crystallizes differently and is thus not homogeneously dispersed in the crystalline phase. This segregation is likely not a consequence of an isotope effect since the Flory–Huggins interaction parameter between the labeled and unlabeled chains is small, $\chi_{HD} = 1.4 \times 10^{-4}$ in the melt, and the product of the interaction parameter with number of repeat units is below the isotope-driven segregation limit, $\chi N \leq 2$. In addition, we do not observe a distinct interphase boundary: the coherent cross sections decay with an exponent of -2.2 in the whole q range; the Porod region with q dependence of $d\Sigma/d\Omega \sim q^{-4}$ is not seen due to the scattering studies being conducted at low q . Furthermore, the cross section data fail to yield a straight line when fitted to a two-phase system proposed by Debye and co-workers in a plot of $d\Sigma/d\Omega^{1-1/2}$ vs q^2 in the low q region.^{74,75} Since we have shown in other studies that the ether-soluble fraction ES-ePP can crystallize (albeit to a very low degree),^{55,72} we attribute the inhomogeneous distribution of the dES-ePP to a differential partitioning of the dES-ePP chains in the amorphous and crystalline domains due to large mismatches in crystallization temperature and kinetics of the d-ES and ePP chains.³⁸ Since the dES chains are likely to contain a low level of crystallizable isotactic sequences, the majority of the chains are excluded and preferentially partitioned in the amorphous domains.

Crystallization-induced phase separation has also been observed by Wignall and co-workers on the blends of linear (high-density) and branched (low-density) polyethylenes from DSC, SANS, and small-angle X-ray scattering (SAXS) experiments.^{76,77} In the molten state, the blends were homogeneous, but upon slow cooling (0.75 °C/min) to room temperature, the components phase segregated due to differences in melting point (~ 20 °C) and structure. Rapid quenching from the melt to -78 °C resulted in extensive cocrystallization to produce a miscible one-phase system. Seki and co-workers have observed similar behavior for isotactic polypropylene/ethylene–propylene blends by SANS and transmission electron microscopy (TEM).⁷⁸ In the molten state, the polymer blends were in a homogeneous single-phase mixture, but at room temperature following a slow crystallization from the melt, the polymer blends were phase separated due to crystallization of the isotactic polypropylene. The ethylene–propylene copolymer, which has much lower crystallization temperature, was excluded from the crystalline phase of the polypropylene chains.

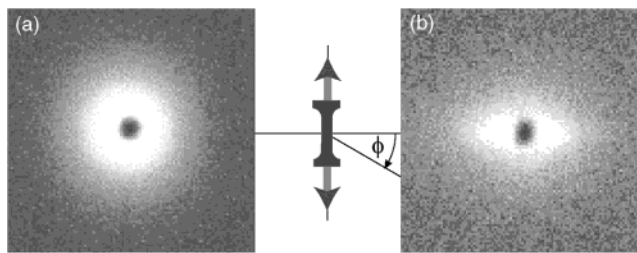


Figure 7. 2-D SANS patterns of d-ES within ePP (dES-ePP): (a). unstretched, and (b). at 300% strain along the vertical direction.

Table 6. SANS Molecular Anisotropy in Crystalline State at 25 °C

sample	orientation parameter $\langle P_2 \rangle$ (%)			
	0%	100%	300%	released ^a
dePP-ePP	0 ± 1			14 ± 1
dES-ePP ^b	0 ± 1	28 ± 2	45 ± 3	17 ± 2
dHS-ePP	0 ± 1			12 ± 1
dHI-ePP	1 ± 1	9 ± 1	24 ± 2	20 ± 1

^a After 1-day released from 300% strain for 1–1.5 h. ^b Crystallization-induced nonhomogeneous mixture; data not to be compared with other fractions.

SANS of ePP-10 under Strain. In an effort to establish the role of the various fractions in the tensile properties of ePP-10, small-angle neutron scattering (SANS) was carried out with a variety of deuterium-labeled ePPs under strain. The experimental protocol for SANS was as follows: the sample was elongated to 100% strain, a SANS image was collected in situ under strain, and then the sample was elongated to 300% strain and a second SANS image was taken. The stress relaxation of the labeled chains was measured after 1–1.5 h at 300% strain. Permanent deformation was monitored from samples held at 300% strain for 1–1.5 h and then released and allowed to relax for 1 day. No induced anisotropy was seen in the SANS patterns in the (control) case of the undoped (fully protonated) ePP sample, even for strains up to 300%.

Figure 7 shows 2-D SANS images of ePP-10 labeled with 5 wt % dES-ePP at room temperature. The SANS image exhibits an isotropic scattering pattern prior to uniaxial tensile stretching. Upon stretching, the labeled chains within ePP exhibit an anisotropic SANS pattern: bright spots develop along the equatorial axis, indicating molecular alignment along the direction of strain. The molecular anisotropy is reported in terms of an orientation parameter $\langle P_2 \rangle$, calculated according to eqs 5–7, and is reported in Table 6. The orientation parameter $\langle P_2 \rangle$ is calculated from azimuthal plots of coherent cross section over a scattering vector range of $0.0106 \text{ \AA}^{-1} < q < 0.0140 \text{ \AA}^{-1}$. Figure 8 shows azimuthal plots of the dES-ePP in this q range.

The deuterated polymer chains are long and semi-flexible, therefore the chain anisotropy cannot be uniquely characterized by a single linear vector represented by $\langle P_2 \rangle$ at a given scattering angle q . The degree of orientation represented by the orientation parameter $\langle P_2 \rangle$ varies with the scattering vector q . The q range for this analysis was deliberately selected to be at the point of the strongest coherent scattering within the 2D pattern for which the resulting analysis is most statistically meaningful. This occurred within a reciprocal space range of $0.0106 \text{ \AA}^{-1} \leq q \leq 0.0140 \text{ \AA}^{-1}$, corresponding to a real space length scale of $450 \text{ \AA} \leq d \leq 590 \text{ \AA}$. This length scales correspond to a linear vector

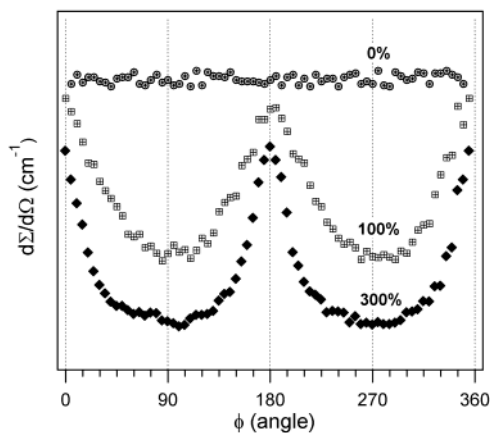


Figure 8. 1-D azimuthal SANS cross section profile of dES-ePP averaged over a q range of $0.0106 \text{ \AA}^{-1} \leq q \leq 0.0140 \text{ \AA}^{-1}$ ($\phi = 0^\circ$ and 180° along the equatorial axis).

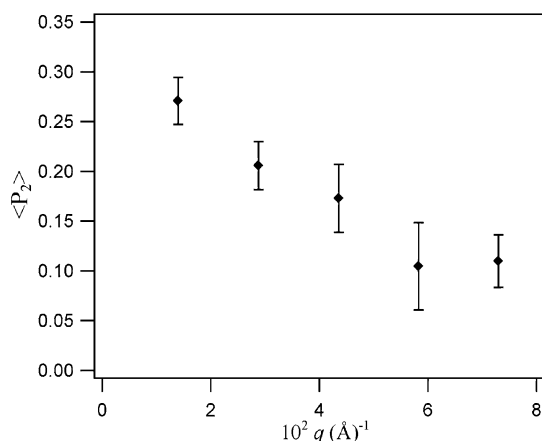


Figure 9. Global orientation parameter $\langle P_2 \rangle$ as a function of reciprocal space vector q for a dES-ePP sample held at a strain deformation of 100%.

representative of an entire chain, and likely represents an average orientation for a group of chains. The variation of $\langle P_2 \rangle$ with q for a dES-ePP sample held under a deformation of 100% is shown in Figure 9, which shows decreasing orientation parameter with increasing scattering vector q .

The results of these experiments (Table 6) reveal that both the dHI-ePP fraction and the dES-ePP fraction show considerable anisotropy when the matrix ePP-10 is held at 100% or 300% strain. In addition all samples show evidence of residual anisotropy when released from a 300% strain, revealing a permanent deformation of the material. This final state retains both macroscopic distortion to the eye and residual molecular orientation in the SANS profiles.

The degree of orientation increases with strain for both the dHI and dES fractions. The orientation parameter for dHI-ePP blend under deformation is rather modest: $\langle P_2 \rangle = 0.09 \pm 0.01$ at 100% strain and $\langle P_2 \rangle = 0.24 \pm 0.02$ at 300% strain. Molecular orientations after 1–1.5 h stress relaxation under 300% strain do not change appreciably. Similar results were obtained from the dES fraction within ePP-10:⁷⁹ $\langle P_2 \rangle = 0.28 \pm 0.02$ at 100% strain and $\langle P_2 \rangle = 0.45 \pm 0.03$ at 300% strain. Significantly after 1 h at 300% strain, the dES-ePP does not show appreciable relaxation despite its low tacticity and crystallinity. One day after release of 1 h of straining at 300%, the orientation relaxes to $\langle P_2 \rangle = 0.17 \pm 0.02$.

The retention of orientation in dHI is expected since this highly crystalline fraction is expected to cocrystallize with ePP-10: the scattering data are consistent with this interpretation. Under strain, the dHI chains are constrained in the crystalline elastomeric network of ePP-10 and some fractions of these chains retain their orientation when held at 300% strain. More surprising perhaps is the observation that the dES fraction also remains anisotropic when held at 100% or 300% strain despite its low crystallinity ($\leq 2\%$ by DSC and WAXS, Table 1). We attribute this residual orientation of the deuterated fraction to the cocrystallization of the dES chains with the more highly tactic components of ePP-10.⁷⁹ This result is corroborated by morphological studies and wide-angle X-ray scattering (WAXS) that the ES fraction of ePP-10 crystallizes by itself and also cocrystallizes with more highly tactic components of ePP-10.^{55,72,79} These data taken together imply that the physical properties of ePP-10 are not simply predicted from the properties of the individual components as described in Figure 1 and Table 2, but instead they imply that the various fractions contribute cooperatively.

The nonzero orientation parameters after releasing from stress signify that the labeled chains retain some permanent orientation. This degree of residual orientation (Table 6) is similar for the doped whole polymer (dePP-ePP) and the intermediate-tacticity fraction (dHS-ePP) with a value of $\langle P_2 \rangle = 0.13 \pm 0.02$, and is $\langle P_2 \rangle = 0.20 \pm 0.01$ for the high-tacticity fraction (dHI-ePP). Compared to $\langle P_2 \rangle = 0.24 \pm 0.02$ at 300% strain, the dHI chains experience only a small decrease in anisotropy upon releasing from stress; the small relaxation of molecular anisotropy suggests that the high tacticity fraction is a primary source of the plastic deformation observed even when it is blended with lower-tacticity fractions. The plastic deformation of the high-tacticity fraction is analogous to that seen in the tensile properties of the neat HI fraction (Figure 1).

Conclusions

Polypropylene synthesized by unbridged 2-arylidene metallocene/MAO catalyst system is a thermoplastic elastomer, which retains its elastomeric properties even at elevated temperature of 50 °C. The tensile properties are a consequence of the combination of both crystalline and amorphous chain sequences: the amorphous sequences are oriented readily under strain, and the crystalline sequences provide a physical network for elastic recovery. The elastomeric polypropylene (ePP) is compositionally heterogeneous and made up of polypropylene chains of varying tacticity, crystallinity, and molecular weight. Each fraction has quite different properties: the high tacticity (HI) fraction exhibits tensile behavior typical of a thermoplastic; the intermediate tacticity (HS) fraction exhibits quite good elastomeric properties similar to ePP, while the low tacticity (ES) fraction acts like a gum elastomer.

Small-angle neutron scattering (SANS) has been used to study the behavior of individually labeled deuterated solvent fractions doped into an elastomeric polypropylene matrix in the melt and crystalline state. In the melt, the deuterated fractions are well-mixed with the elastomeric polypropylene matrix and constitute a one-phase system. In the crystalline state at 25 °C following a slow crystallization from the melt, the majority of the deuterated doped fractions (dePP-ePP, dHS-ePP, and

dHI-ePP) are homogeneously mixed in the ePP matrix except for the low tacticity fraction (dES-ePP) which appears to be inhomogeneously mixed. The slow crystallization from the melt induces a partitioning of the d-ES chains into less crystalline domains.

The role of each fraction residing within ePP under tensile deformation was studied using SANS. The high tacticity fraction (dHI-ePP) showed plastic deformation with very little molecular anisotropy relaxation upon releasing from stress. The intermediate tacticity fraction (dHS-ePP) exhibits similar permanent anisotropy behavior as the whole d-ePP (dePP-ePP); this suggests that the elasticity in ePP may be dominated by the intermediate tacticity fraction. The low tacticity fraction (dES-ePP), despite its low crystallinity, can cocrystallize with the crystalline matrix. SANS shows that the molecular anisotropy of d-ES chains within ePP does not relax appreciably when held under strain.

Acknowledgment. G.G.F., R.M.W., and W.W. acknowledge support from the National Science Foundation (DMR-9910386). We acknowledge the support of the Stanford Synchrotron Radiation Laboratory (SSRL) in providing facilities used in these experiments and for Thomas Hostetler of SSRL for the construction of the oven and motor mount onto the tensile testing device; this work was supported by Department of Energy Contract DE-AC03-76SF00515. We acknowledge Steve Cheatham, at Varian Application Lab, for NMR analysis. We acknowledge the support of the National Institute of Standards and Technology, U.S. Department of Commerce, in providing the neutron facilities used in this work, supported by the National Science Foundation under Agreement No. DMR-9423101, and thank the station scientists, Boualem Hammouda and Kathleen Barnes, for their assistance. The authors also acknowledge partial support for this work from the NSF Center for Polymer Interfaces and Macromolecular Assemblies (CPIMA) under cooperative agreement DMR-9400354 and BP Chemical Co.

References and Notes

- Jebens, A. *Polypropylene Resins*, SRI International: Menlo Park, CA, 1997.
- Natta, G.; Mazzanti, G.; Crespi, G.; Moraglio, G. *Chim. Ind.* **1957**, *39*, 275–283.
- Natta, G. *J. Polym. Sci.* **1959**, *34*, 531–549.
- Collette, J. W.; Ovenall, D. W.; Buck, W. H.; Ferguson, R. C. *Macromolecules* **1989**, *22*, 3858–3866.
- Collette, J. W.; Tullock, C. W. US Patent 4,335,225, 1982.
- Collette, J. W.; Tullock, C. W.; MacDonald, R. N.; Buck, W. H.; Su, A. C. L.; Harrel, J. R.; Mulhaupt, R.; Anderson, B. C. *Macromolecules* **1989**, *22*, 3851–3858.
- Tullock, C. W.; Tebbe, F. N.; Mulhaupt, R.; Ovenall, D. W.; Setterquist, R. A.; Ittel, S. D. *J. Polym. Sci., Part A: Polym. Chem.* **1989**, *27*, 3063–3081.
- Ittel, S. D. *J. Macromol. Sci. Chem.* **1990**, *A27*, 9–11.
- Tullock, C. W.; Mulhaupt, R.; Ittel, S. D. *Makromol. Chem., Rapid Commun.* **1989**, *10*, 19–23.
- Job, R. C.; Haas, D. F. US Patent 5,118,768, 1992.
- Job, R. C. US Patent 5,089,573, 1992.
- Chen, R.; Xie, M. R.; Wu, Q.; Lin, S. G. *J. Polym. Sci., Part A: Polym. Chem.* **2000**, *38*, 411–415.
- Kuhl, O.; Koch, T.; Somoza, F. B.; Junk, P. C.; Hey-Hawkins, E.; Plat, D.; Eisen, M. S. *J. Organomet. Chem.* **2000**, *604*, 116–125.
- Longo, P.; Amendola, A. G.; Fortunato, E.; Boccia, A. C.; Zambelli, A. *Macromol. Rapid Commun.* **2001**, *22*, 339–344.
- Mansel, S.; Perez, E.; Benavente, R.; Perena, J. M.; Bello, A.; Roll, W.; Kirsten, R.; Beck, S.; Brintzinger, H. H. *Macromol. Chem. Phys.* **1999**, *200*, 1292–1297.
- Nedorezova, P. M.; Tsvetkova, V. I.; Bravaya, N. M.; Savinov, D. V.; Optov, V. A. *Polym. Sci. Ser. A* **2000**, *42*, 573–579.
- Schmidt, R.; Alt, H. G. *J. Organomet. Chem.* **2001**, *621*, 304–309.
- Yoon, J. S.; Lee, Y. S.; Park, E. S.; Lee, I. M.; Park, D. K.; Jung, S. O. *Eur. Polym. J.* **2000**, *36*, 1271–1275.
- Resconi, L.; Piemontesi, F.; Lin-Chen, Y. US Patent 5,747,621, 1998.
- Sassmannshausen, J.; Bochmann, M.; Rosch, J.; Lilge, D. *J. Organomet. Chem.* **1997**, *548*, 23–28.
- Chien, J. C. W.; Llinas, G. H.; Rausch, M. D.; Lin, Y. G.; Winter, H. H.; Atwood, J. L.; Bott, S. G. *J. Polym. Sci., Part A: Polym. Chem.* **1992**, *30*, 2601–2617.
- Mallin, D. T.; Rausch, M. D.; Lin, Y. G.; Dong, S.; Chien, J. C. W. *J. Am. Chem. Soc.* **1990**, *112*, 2030–2031.
- Llinas, G. H.; Dong, S. H.; Mallin, D. T.; Rausch, M. D.; Lin, Y. G.; Winter, H. H.; Chien, J. C. W. *Macromolecules* **1992**, *25*, 1242–1253.
- Chien, J. C. W.; Llinas, G. H.; Rausch, M. D.; Lin, G. Y.; Winter, H. H.; Atwood, J. L.; Bott, S. G. *J. Am. Chem. Soc.* **1991**, *113*, 8569–8570.
- Cheng, H. N.; Babu, G. N.; Newmark, R. A.; Chien, J. C. W. *Macromolecules* **1992**, *25*, 6980–6987.
- Gauthier, W. J.; Corrigan, J. F.; Taylor, N. J.; Collins, S. *Macromolecules* **1995**, *28*, 3771–3778.
- Gauthier, W. J.; Collins, S. *Macromolecules* **1995**, *28*, 3779–3786.
- Bravakis, A. M.; Bailey, L. E.; Pigeon, M.; Collins, S. *Macromolecules* **1998**, *31*, 1000–1009.
- Dietrich, U.; Hackmann, M.; Rieger, B.; Klinga, M.; Leskelae, M. *J. Am. Chem. Soc.* **1999**, *121*, 4348–4355.
- Kukral, J.; Lehmus, P.; Feifel, T.; Troll, C.; Rieger, B. *Organometallics* **2000**, *19*, 3767–3775.
- Dreier, T.; Erker, G.; Froehlich, R.; Wibbeling, B. *Organometallics* **2000**, *19*, 4095–4103.
- Coates, G. W.; Waymouth, R. M. *Science* **1995**, *267*, 217–219.
- Hauptman, E.; Waymouth, R. M.; Ziller, J. W. *J. Am. Chem. Soc.* **1995**, *117*, 11586–11587.
- Bruce, M. D.; Coates, G. W.; Hauptman, E.; Waymouth, R. M.; Ziller, J. W. *J. Am. Chem. Soc.* **1997**, *119*, 11174–11182.
- Kravchenko, R.; Masood, A.; Waymouth, R. M. *Organometallics* **1997**, *16*, 3635–3639.
- Petoff, J. L. M.; Bruce, M. D.; Waymouth, R. M.; Masood, A.; Lal, T. K.; Quan, R. W.; Behrend, S. J. *Organometallics* **1997**, *16*, 5909–5916.
- Bruce, M. D.; Waymouth, R. M. *Macromolecules* **1998**, *31*, 2707–2715.
- Carlson, E. D.; Krejchi, M. T.; Shah, C. D.; Terakawa, T.; Waymouth, R. M.; Fuller, G. G. *Macromolecules* **1998**, *31*, 5343–5351.
- Hu, Y. R.; Krejchi, M. T.; Shah, C. D.; Myers, C. L.; Waymouth, R. M. *Macromolecules* **1998**, *31*, 6908–6916.
- Kravchenko, R.; Masood, A.; Waymouth, R. M.; Myers, C. L. *J. Am. Chem. Soc.* **1998**, *120*, 2039–2046.
- Kravchenko, R.; Waymouth, R. M. *Macromolecules* **1998**, *31*, 1–6.
- Lin, S.; Hauptman, E.; Lal, T. K.; Waymouth, R. M.; Quan, R. W.; Ernst, A. B. *J. Mol. Catal. A: Chem.* **1998**, *136*, 23–33.
- Petoff, J. L. M.; Agoston, T.; Lal, T. K.; Waymouth, R. M. *J. Am. Chem. Soc.* **1998**, *120*, 11316–11322.
- Waymouth, R. M.; Kravchenko, R.; Bendig, L. L.; Moore, E. J.; Myers, C. L.; Quan, R. W.; Ernst, A. B. US Patent 6,160,064, 2000.
- Witte, P.; Lal, T. K.; Waymouth, R. M. *Organometallics* **1999**, *18*, 4147–4155.
- Carlson, E. D.; Fuller, G. G.; Waymouth, R. M. *Macromolecules* **1999**, *32*, 8100–8106.
- Carlson, E. D.; Fuller, G. G.; Waymouth, R. M. *Macromolecules* **1999**, *32*, 8094–8099.
- Hu, Y. R.; Carlson, E. D.; Fuller, G. G.; Waymouth, R. M. *Macromolecules* **1999**, *32*, 3334–3340.
- Lin, S.; Waymouth, R. M. *Macromolecules* **1999**, *32*, 8283–8290.
- Petoff, J. L. M.; Myers, C. L.; Waymouth, R. M. *Macromolecules* **1999**, *32*, 7984–7989.
- Tagge, C. D.; Kravchenko, R. L.; Lal, T. K.; Waymouth, R. M. *Organometallics* **1999**, *18*, 380–388.
- Boue, F. *Adv. Polym. Sci.* **1987**, *82*, 47–101.
- Lohse, D. J. *Rubber Chem. Technol.* **1994**, *67*, 367–383.
- Zirkel, A.; Urban, V.; Richter, D.; Fetters, L. J.; Huang, J. S.; Kampmann, R.; Hadjichristidis, N. *Macromolecules* **1992**, *25*, 6148–6155.

- (55) (a) Wiyatno, W.; Pople, J. A.; Gast, A. P.; Waymouth, R. M.; Fuller, G. G. *Macromolecules* **2002**, *35*, 8488–8497. (b) Wiyatno, W.; Pople, J. A.; Gast, A. P.; Waymouth, R. M.; Fuller, G. G. *Macromolecules* **2002**, *35*, 8498–8508.
- (56) Wiyatno, W.; Chen, Z.-R.; Liu, Y.; Waymouth, R. M.; Krukonic, V.; Brennan, K. submitted to *Macromolecules* 2002.
- (57) Wunderlich, B. *Macromolecular Physics*; Academic Press: New York, 1976. Vol. 2: Crystal Nucleation, Growth, Annealing.
- (58) Daoud, M.; Cotton, J. P.; Farnoux, B.; Jannink, G.; Sarma, G.; Benoit, H.; Duplessix, R.; Picot, C.; Gennes, P. G. D. *Macromolecules* **1975**, *8*, 804–818.
- (59) Maconnachie, A.; Richards, R. W. *Polymer* **1978**, *19*, 739–762.
- (60) Hayashi, H.; Flory, P. J.; Wignall, G. D. *Macromolecules* **1983**, *16*, 1328–1335.
- (61) De Gennes, P. G. *Scaling Concepts in Polymer Physics*; Cornell University Press: Ithaca, NY, 1979.
- (62) Glatter, O.; Kratky, O.; Editors. *Small-Angle X-ray Scattering*; Academic Press: New York, 1982.
- (63) Debye, P. *J. Phys. Colloid Chem.* **1947**, *51*, 18–32.
- (64) Wignall, G. D. *Encycl. Polym. Sci. Eng.* **1987**, *10*, 112–184.
- (65) Alamo, R. G.; Londono, J. D.; Mandelkern, L.; Stehling, F. C.; Wignall, G. D. *Macromolecules* **1994**, *27*, 411–417.
- (66) Bassett, D. C.; Editor. *Developments in Crystalline Polymers-2*; Kluwer Academic Publishers, Dordrecht, The Netherlands, 1988.
- (67) Pople, J. A.; Mitchell, G. R. *Liq. Cryst.* **1997**, *23*, 467–473.
- (68) Lacey, D.; Beattie, H. N.; Mitchell, G. R.; Pople, J. A. *J. Mater. Chem.* **1998**, *8*, 53–60.
- (69) Pople, J. A.; Mitchell, G. R.; Chai, C. K. *Polymer* **1996**, *37*, 4187–4191.
- (70) Myers, C. A.; Allen, C.; Ernst, A.; Naim, H. *Society of Plastics Engineers (SPE) Conference Proceedings*, Society of Plastics Engineers (SPE) New York, 1999; Vol. 55, Session M10.
- (71) The tensile properties were also tested on compression-molded samples retained for 1 year at room temperature. The tensile properties of the 1-year-old samples were very similar to those tested 1 day after compression molding.
- (72) Schonherr, H.; Wiyatno, W.; Pople, J. A.; Frank, C. W.; Fuller, G. G.; Gast, A. P.; Waymouth, R. M. *Macromolecules* **2002**, *35*.
- (73) Alamo, R. G.; Graessley, W. W.; Krishnamoorti, R.; Lohse, D. J.; Londono, J. D.; Mandelkern, L.; Stehling, F. C.; Wignall, G. D. *Macromolecules* **1997**, *30*, 561–566.
- (74) Debye, P.; Anderson, H. R., Jr.; Brumberger, H. *J. Appl. Phys.* **1957**, *28*, 679–683.
- (75) Debye, P.; Bueche, A. M. *J. Appl. Phys.* **1949**, *20*, 518–525.
- (76) Wignall, G. D.; Alamo, R. G.; Londono, J. D.; Mandelkern, L.; Kim, M. H.; Lin, J. S.; Brown, G. M. *Macromolecules* **2000**, *33*, 551–561.
- (77) Wignall, G. D.; Londono, J. D.; Lin, J. S.; Alamo, R. G.; Galante, M. J.; Mandelkern, L. *Macromolecules* **1995**, *28*, 3156–3167.
- (78) Seki, M.; Nakano, H.; Yamauchi, S.; Suzuki, J.; Matsushita, Y. *Macromolecules* **1999**, *32*, 3227–3234.
- (79) The order parameters of dES-ePP cannot be directly compared to those of dHI-ePP because the d-ES fraction, unlike its d-HS and d-HI counterparts, is not homogeneously distributed within ePP-10 in its semicrystalline form at 25°C. Nevertheless, there is some constraint that prevents the d-ES fraction from relaxing when held at strain, and therefore, some cooperative behavior between the d-ES fraction and its host matrix.

MA020477Q